

1 Self-assembly and Sensor Response of Photosynthetic Reaction Centers on 2 Screen-printed Electrodes.

3
4 Vijayender Bhalla⁺, Valter Zazubovich^{*}

5
6 *Department of Physics, Concordia University, 7141 Sherbrooke St. West, Montreal, Quebec*
7 *H4B 1R6, Canada*

8 9 Abstract

10 Photosynthetic reaction centers were immobilized onto gold screen-printed electrodes (Au-SPE)
11 using a self-assembled monolayer (SAM) of mercaptopropionic acid (MPA) which was
12 deliberately defective in order to achieve effective mediator transfer to the electrodes. The pure
13 Photosystem II (PS II) cores from spinach immobilize onto the electrodes very efficiently but fair
14 badly in terms of photocurrent response (measured using duroquinone as the redox mediator).
15 The cruder preparation of PS II known as BBY particles performs significantly better under the
16 same experimental conditions and shows a photocurrent response of 20 to 35 nA (depending on
17 preparation) per screen-printed electrode surface (12.5 mm²). The data was corroborated using
18 AFM, showing that in the case of BBY particles a defective bilayer is indeed formed, with
19 grooves spanning the whole thickness of the layer enhancing the possibility of mass transfer to
20 the electrodes and enabling biosensing. In comparison, the PS II core layer showed ultra-dense
21 organization, with additional formation of aggregates on top of the single protein layer, thus

| * Corresponding author; phone (1-514) 848-2424 #5050; fax (1-514) 848-2828; e-mail: vzazubov@alcor.concordia.ca .1

⁺Present Address: Biosensors Laboratory, Institute of Microbial Technology, Sector 39-
A Chandigarh India 160036; ykbhalla@imtech.res.in

22 blocking mediator access to the electrodes and/or binding sites. The defective monolayer
23 biosensor with BBY particles was successfully applied for the detection of photosynthesis
24 inhibitors, demonstrating that the inhibitor binding site remained accessible to both the inhibitor
25 and the external redox mediator. Biosensing was demonstrated using picric acid and atrazine.
26 The detection limits were 1.15 nM for atrazine and 157 nM for picric acid.

27

28 **Keywords:** Photosynthetic reaction centers; Gold screen printed electrode; Self-assembled
29 monolayer; Herbicide detection; Atrazine; Picric acid.

| * Corresponding author; phone (1-514) 848-2424 #5050; fax (1-514) 848-2828; e-mail: vzazubov@alcor.concordia.ca

+Present Address: Biosensors Laboratory, Institute of Microbial Technology, Sector 39-
A Chandigarh India 160036; ykbhalla@imtech.res.in

30 **1. Introduction**

31 Biosensing, one of the many possible practical applications of biomolecules, requires the
32 controlled immobilization of biomolecules in close contact with electrochemical transducers.
33 Self-assembled monolayers (SAM) provide a unique tunable platform since the thickness of the
34 organic layers and surface properties are adjustable to suit different sensing applications [1]. The
35 organic molecules forming SAM feature different anchor groups that can be used to attach
36 various classes of biomolecules [2]. They also provide some level of control over packing
37 density at the surface [3]. Generally, use of SAMs allows the biochemical reaction to proceed in
38 a more controlled manner thus enhancing biosensing parameters [4].

39 One common approach towards selective herbicide detection is based on the use of
40 antibodies [5]. However, generation of antibodies against small molecules is tedious and time
41 consuming process, and requires animal models to raise the antibodies. Antibody-based detection
42 may also face problems due to cross-reactivity of antibodies with similar compounds [6].
43 Antibodies are fairly large objects, especially compared to small herbicide molecules;
44 additionally, blocking in immunoassays is a complex problem that has to be addressed before
45 any useful data is obtained. Summarizing, there is an apparent need to continue looking for
46 alternative approaches, one of them being to employ the natural photosynthesis machinery for
47 detection purposes. Photosynthetic biosensors are capable of detecting a broad spectrum of
48 herbicides and have generated a lot of interest as an alternative to antibody-based biosensing.
49 Whole photosynthetic organisms [7], as well as bacterial reaction centers [8], have been used for
50 this purpose. The most common version makes use of Photosystem II (PS II), the photosystem
51 that is also responsible for water splitting and oxygen production. The initial reports on PS II-
52 based herbicide biosensors employed electrochemical flow cells with PS II in suspension [9] or

53 immobilized with the help of different substances [10-12]. Clark electrode-based setup that
54 monitors changes in oxygen evolution activity of the PS II was used in [13]. More recent reports
55 again focused on amperometric detection, with the photosynthetic material entrapped in gel
56 matrices on top of the electrodes [14-17]. Combining electrochemical and optical detection has
57 been recently reported in [18]. In PS II the illumination induces charge separation, with electron
58 eventually traveling to mobile plastoquinone Q_B . In vivo the latter accepts two electrons (and
59 two protons), transforms to quinol and carries the electrons away. The mechanism of inhibition
60 of PS II by herbicides in vivo involves herbicide molecules attaching to the Q_B binding site and
61 preventing plastoquinone from binding. The exposure of the PS II-based biosensor to the
62 inhibitor results in a decrease of the photoinduced current in an electrical circuit containing the
63 photosynthetic reaction centers, because the mediator (replacing plastoquinone) cannot bind to
64 the Q_B site.

65 Although entrapping photosynthetic materials in gels allows for reasonable accessibility
66 due to the porous nature of the matrix, it has some inherent limitations. The main limitations are
67 due to swelling or contraction of gels with time, poor adhesion to the electrodes, and the stress of
68 fluid movement that may lead to washing off of certain materials trapped in the matrix. The
69 diffusion coefficient of mediators and herbicides in different gels, polymers and other matrices is
70 also a limiting factor. Covalent immobilization using BSA-glutaraldehyde has been found to be
71 better than other schemes as it is a simple one-step procedure based on cross-linking of amines
72 that results in a very stable matrix system on top of the electrodes [16,18]. Another procedure,
73 resulting in preservation of photosynthetic activity for somewhat longer time involves
74 immobilization using poly(vinylalcohol) bearing styrylpyridinium groups (PVA-SbQ) [19].

75 The immobilization of photosynthetic materials in a monolayer fashion is quite
76 challenging and has been of interest for various applications, including bioelectrocatalytic fuel
77 cells [20]. The immobilization of PS II with the help of SAMs has been carried out using
78 Histidine-tagged PS II that attaches to nickel on the NTA (nitrilotriacetic acid) SAM [21]. This
79 technology requires genetic engineering to introduce the histidine tag into the PS II. Moreover,
80 Ni-NTA-terminated SAM preparation on gold electrodes involves a multistep protocol. Thus,
81 although this method leads to immobilization of the reaction centers in a uniformly-oriented
82 fashion, the mass transfer to the electrodes becomes limited due to multiple layering steps
83 effectively insulating the electrodes. Maly et al. [22] studied this topic and suggested deliberately
84 creating defect structures using BSA in the PS II sensing bilayer to achieve increased mass
85 transfer efficiency to the electrodes while working with NTA-SAM as the linker molecule.
86 However, this approach could lead to decreased current due to the co-immobilization of BSA on
87 the sensing surface.

88 In the present report we suggest a simpler approach that makes use of carboxylic acid
89 anchoring groups of MPA SAM on gold screen-printed electrode (Au SPE) surface to bind
90 native PS II reaction centers or membrane fragments for unique biointerface development. The
91 MPA films are known to exhibit many pinhole defects [23]. We utilize these pinhole defects to
92 achieve effective mass transfer to the electrodes.

93

94 **2. Experimental**

95 All chemicals were purchased from Sigma-Aldrich (USA). Organic baby spinach leaves
96 were purchased from the local food suppliers. Buffer compositions were as follows:

97 Homogenizing buffer: 20 mM MES (pH 6.0), 15 mM NaCl, 5 mM CaCl₂. Measuring buffer: 15
98 mM 2-(N-morpholino) ethanesulfonic acid (MES), pH 6.5, 0.5 M mannitol, 0.1 M NaCl, 5 mM
99 MgCl₂, and 5 x 10⁻⁵ M chloramphenicol (supplemented with 0.2 mM DQ).

100

101 **2.1 Isolation of PS II-containing particles**

102 The BBY particles [24] refer to PS II-enriched membrane fragments. The BBY particles
103 are mostly devoid of Photosystem I, but still retain the oxygen evolving capacity and some lipid
104 membranes within which the hydrophobic mediator can travel and reach its binding site. Both
105 core and peripheral antenna complexes of PS II are retained. BBY particles were obtained after
106 treatment of thylakoids with Triton X-100 at a final concentration of 25 mg per mg Chl and
107 repeated centrifugation for 25 min at 40,000 g) in homogenizing buffer. The chlorophyll
108 concentration for all purposes was determined by the method of Arnon [25].

109 The PS II core particles were prepared similarly to [26]. These particles constitute the
110 minimal PS II preparation still retaining the oxygen-evolving capacity, and consist of the PS II
111 reaction center, as well as CP43 and CP47 core antenna complexes. Note that in this case the
112 photosynthetic protein is encased into the detergent micelle and the original thylakoid membrane
113 is not retained.

114

115 **2.2 Surface preparation procedures**

116 A 2 mM MPA solution prepared in a 75/25% ethanol/water mixture (vol/vol) was used
117 for the formation of SAMs. Gold surfaces were incubated for 1 hour, in the dark, and then rinsed
118 with ethanol. After that sonication in ethanol/water was carried out for 5 minutes in order to
119 remove physisorbed thiols from the gold surface. The surfaces were further washed with

120 deionized water and dried with nitrogen. For AFM investigations (see Sections 2.4 and 3.2), the
121 SAM was formed not on a screen-printed electrode but on gold substrate (100 nm thickness)
122 prepared by electron beam evaporation on a silicon dioxide chip with a 5 nm titanium stick layer.
123 The gold surface was cleaned in a piranha solution (mixture of 3:1 of H₂SO₄ and H₂O₂) for 30
124 min before deposition of SAM.

125 After SAM formation, the electrodes were treated for 10 minutes with a mixture of NHS
126 – N-hydroxysuccinimide (0.05 M) and EDC – Ethyl-Dimethyl-aminopropyl Carbodiimide (0.2
127 M) solutions in distilled deionized water. As a zero-degree cross-linking agent EDC does not
128 introduce any additional chemical groups between the conjugating molecules. EDC reacts with
129 carboxyl groups of the MPA SAM, forming an amine-reactive *o*-acylisourea intermediate. This
130 intermediate in turn can react with amines of the photosynthetic material forming amide bonds
131 and releasing isourea by-product [27]. A further incubation (6 hours at 4 °C in the dark) was
132 carried out with the PS II particle suspension. The electrodes were carefully washed in MES
133 buffer and dried with nitrogen after each incubation step.

134

135 **2.3 Photo-electrochemical Measurements**

136 Gold screen-printed electrodes were purchased from DropSens Inc. (model DRP-220).
137 The electrode assembly consists of a gold working electrode (area 12.57 mm²) and a gold
138 counter electrode. The reference electrodes and electrical contacts were made of silver and
139 screen printed on a ceramic substrate 3.4 x 1 x 0.05 cm (length x width x thickness). All potential
140 values are reported with respect to silver pseudo reference electrode. The electrochemical

141 response of the electrodes with and without immobilized material was investigated using the CHI
142 630C electrochemical workstation.

143 The schematics of the biosensor are presented in Figure 1. For amperometric detection of
144 photosynthesis inhibitors the *I-t* curves were measured at room temperature, with 50 μ l droplets
145 of the measuring buffer placed onto the working area covering the three electrodes. Duroquinone
146 (DQ; 0.2 mM) was used as a mediator in these experiments and, respectively, the working
147 electrode was polarized at 0.62 V [16,28]. Quinones are used as mediators in PS II-based
148 herbicide biosensors due to their similarity to plastoquinone which binds to the Q_B site in vivo.
149 DQ in particular was employed as a mediator also in [13,14,17]. Other mediators used in PS-II
150 based biosensors include 2,5-dichlorobenzoquinone [11], 2,6-dichlorophenolindophenol [18] and
151 ferricyanide [10,16,28]. Ferricyanide, although providing the largest photocurrents, is clearly not
152 specific for the Q_B site [16,28]. A 7 mW laser diode with 675 nm wavelength (near the peak of
153 the PS II Q_y absorption band) was used for illumination. In the absence of light only small dark
154 current is registered. Illuminating the sensor leads to a significant increase in the detected current
155 which is due to light-induced charge separation in the PS II. Turning the light off results in the
156 return of the current to the pre-illumination levels (See also sections 3.1 and 3.3). Addition of
157 photosynthesis inhibitors results in a decrease of the magnitude of the photo-induced current
158 peak. [Suggested location of Fig.1)]

159

160 **2.4 AFM Characterization**

161 AFM studies were performed in order to assess the quality of SAM formation and
162 photosynthetic material immobilization. The AFM images were obtained in air, while operating
163 in tapping mode, using a Digital Instruments Multimode AFM with a standard sharpened Si₃N₄

164 tip (cantilever resonant frequency was 300 kHz). The images were collected with high resolution
165 (512 points per line) at a scan rate of 1–2 Hz. Raw images were only processed for background
166 removal (flattening) using the AFM manufacturer’s software.

167

168 **3. Results and Discussion**

169 **3.1 Electrochemical and photo-electrochemical characterization**

170 The gold screen printed electrodes were used for thiol films formation. Not many reports
171 have previously focused on thiol-Au films formation on screen printed electrodes; notable
172 exceptions include [29,30]. Our goal was to form a non-insulating SAM (that would allow free
173 movement of the mediator to the electrode surface) using short chain alkanethiols. It is well
174 known that as the chain length decreases, the degree of order of SAM’s decreases as well,
175 together with the packing density and surface coverage [31]. The well-known redox curve of
176 potassium ferrocyanide on gold electrode surface is presented in Figure 2 (solid curve). This
177 curve can be compared with the curve measured for the electrodes covered with MPA SAM
178 (dashed curve). The response is clearly decreased. On the other hand, the features of the cyclic
179 voltammograms demonstrate that the thiol SAM is not perfectly insulating as the redox reaction
180 of ferrocyanide is still accessible [32]. For comparison, almost no current is detected in case of
181 highly-ordered SAM [33]. [Suggested location of Figure 2]

182 The proper immobilization of PS II core particles on MPA SAM was confirmed by
183 observing the redox reaction for the various cofactors naturally present in the PS II structure. The
184 cyclic voltammetry (CV) technique was used to characterize development of proper biointerface
185 on SPE. The CV scans of immobilized core particles were obtained in MES buffer pH 6.5 and
186 showed a reversible peak and a non-reversible peak when investigated using screen printed Au

187 electrodes with a silver pseudo-reference electrode (Supplemental Information, Fig. S1). A
188 reversible peak at redox midpoint potential of -0.086 V can be ascribed to the (native) quinones
189 (Q/Q^-), and the irreversible peak at ~ 0.22 V can be ascribed to the tetramanganese (Mn_4) cluster
190 which shows that it is intact and accessible to the electrochemical reaction as described earlier
191 [34]. The fact that this reaction is observed indicates close contact between PS II and the
192 electrodes due to the short chain length of the SAM material.

193 Figure 3 compares the photocurrent signal measured as the reoxidation of the
194 duroquinone (DQ) mediator at 0.62 V for the immobilized BBY sample in the cases of BSA-
195 glutaraldehyde matrix system (A) and SAM (B), solid curves. The photocurrent signal is higher
196 in case of SAM as compared to matrix-based immobilization for the same area of the electrode.
197 As can be seen in the picture there is a significant difference in the sensor's response in these two
198 cases. The difference arises mainly from the re-oxidation rate of the reduced mediator. In the
199 case of immobilization of PS II on the SAM layer the mediator can access the electrode surface
200 more easily. In the case of the matrix system, on the other hand, the speed of this process is
201 limited by the diffusion rate of the mediator in the gel matrix and the reoxidation process takes
202 longer [35]. The dotted curve in the frame B is an example of the signal in the presence of
203 photosynthesis inhibitor. Surprisingly, the photocurrent signal in the case of PS II cores was 1.00
204 ± 0.75 nA only, significantly smaller than for BBY particles. [Suggested location of Figure 3]

205 Concerning the biosensor stability, in the case of BBY particles it took about 24 hours for
206 the photocurrent signal to be reduced by half (see Supplemental Information, Fig. S2). The
207 photocurrent did not show significant decay in the first 2 hours, most probably due to the
208 stabilization effect of the natural lipid membrane environment.

209

210 **3.2 Atomic force microscopy of surfaces**

211 The photocurrent generation properties observed using duroquinone as a mediator were
212 significantly different for BBY particles and PS II core preparations. AFM investigation allowed
213 us to shed more light on the possible reasons of these differences. The AFM imaging was
214 conducted using flat evaporated gold surface rather than the surface of the screen-printed
215 electrodes. Thus, we managed to elucidate the fine details of SAM formation and photosynthetic
216 material binding which could otherwise be partially masked by the higher surface roughness of
217 the screen-printed electrodes. According to SEM images presented at manufacturer's website
218 (<http://www.dropsens.com>), the surface of the screen-printed electrodes used in this work features
219 granules of the size of $\sim 2 \mu\text{m}$, not very suitable for detailed AFM investigation. On the other
220 hand, this is at least an order of magnitude larger than features described below. Thus, we
221 believe that the details of SAM formation and PS II immobilization do not differ drastically
222 between evaporated gold surface and screen-printed electrode. The quality of the SAM and of
223 the bio-layer can be characterized by root mean square (RMS) roughness. Table 1 summarizes
224 the RMS roughness values for bare surface as well as the surfaces after various modifications.
225 The RMS roughness for the bare gold surface was 1.05 ± 0.1 nm. The deposition of the SAM
226 led to a small increase in the surface roughness to 1.85 ± 0.25 nm. Figure 4 shows the AFM
227 images of the bare gold surface and the MPA SAM on the gold surface. The topology of a nicely
228 formed SAM almost perfectly follows the gold layer's corrugation, although defects in SAM
229 such as cracks or patches would contribute to an increase in RMS roughness [36]. The
230 immobilization of the photosynthetic complexes leads to a significant increase of the roughness.
231 The RMS roughness increases to 21.9 nm with the immobilization of PS II core particles and to
232 8.67 nm for BBY membranes. The larger roughness in case of the pure PS II core sample is most

233 likely due to cluster formation as illustrated in the schematic accompanying Figure 5A. For BBY
234 membranes we do not observe aggregate formation upon immobilization. The thickness of the
235 layer is approximately 10 nm, in agreement with values previously reported for these particles
236 using AFM imaging [22]. The AFM image of the immobilized PS II core particles on the MPA
237 SAM (Figure 5A) show some repeatable features with the size (in the plane of the layer) of
238 approximately 50 nm, as well as some objects of larger size, 100 nm and beyond. The height of
239 the former features is approximately 10 nm. These must be the clusters of PS II core particles
240 since individual PS II core dimers have been reported to have much smaller size, namely 20.6 x
241 13.1 nm, with thickness varying from 6.0 nm on the periphery of the complex to 9.1 nm in the
242 RC region [37]. In [37] the thickness of the detergent layer around the hydrophobic surface of
243 the protein was estimated at 1.6 nm only. Incidentally, in an earlier report the AFM images
244 contained some 40-60 nm features for histidine-modified PS II immobilized on nickel-
245 nitriloacetic acid (Ni-NTA) SAM [22]. Another report described smaller features whose size was
246 consistent with that of the PS II dimers [38]. The high purity and homogeneity of this protein
247 preparation allows immobilizing it in a very dense manner thus most likely completely blocking
248 mediator access to the electrodes or the Q_B sites. (Although the PS II core samples were
249 detergent-solubilized, one also cannot exclude a possibility that hydrophobicity of the
250 complexes, isolated from natural membranes, contributes to their aggregation.) This result is in
251 accordance with those by other researchers who found higher protein densities to interfere with
252 biosensor assays mainly by interfering with the diffusion of the analyte to the enzyme or by
253 hindering electron transfer to the electrode surface [39]. In addition, higher protein loading on
254 the surface, particularly for enzymes, has been shown to neutralize active sites or alter the
255 morphology of the enzyme through mutual interactions [40]. Thus, the poor performance of this

256 preparation, in our case, was ascribed to the higher protein density, in agreement with the results
257 of other researchers who found high protein densities to be a limiting factor in the performance
258 of biosensors [41-43]. It is also possible that detergent micelle, as opposed to native thylakoid
259 membrane present in BBY particles, is preventing the access of the mediator to the Q_B site.

260 In the case of BBY particles the membrane fragments successfully immobilize on the
261 surface but not in an ultra-dense manner. The image in Figure 5B shows heterogeneous features.
262 It has both areas (marked with a square) with uniform immobilization of relatively small
263 membrane fragments, as well as regions (outside of the square) with large membrane fragments
264 on top of the gold surface and possibly on top of each other. The presence of the natural
265 membrane environment in case of BBY particles likely allows the hydrophobic mediator to gain
266 better access to the Q_B binding site. The presence of nanogaps in the film allows the reduced
267 mediator in solution to gain better access to the electrode surface as shown in schematic
268 accompanying Figure 5B. The smallest particles present in the AFM image in Figure 5B appear
269 to be approximately 25-30 nm, consistent with the size of the dimeric PS II supercomplexes
270 containing peripheral antenna [37]. Figure 6 directly compares the cross-section features (along
271 the lines present in Figure 5 A and B, respectively) for the two sample preparations. In case of
272 the PS II cores the features repeat with the period of approximately 100 nm, with occasional
273 larger aggregate formation. In case of BBY sample the grooves are observed in the bilayer,
274 spanning the total thickness of the bilayer i.e. ~10 nm. Thus in the latter case there is ample
275 opportunity for mediator to gain access to the electrode surface. [Suggested location for Figures
276 4, 5, 6]

277

278 **3.3 Detection of photosynthesis inhibitors**

279 Herbicides inhibit photosynthesis by interrupting electron transfer at the quinone-
280 reducing site of PS II. In vivo herbicides compete with the plastoquinone for its Q_B binding site
281 on the D1 protein, thus leading to disruption of electron transfer from Q_A to Q_B and further along
282 the electron transport chain. In our experiments the herbicide binding to the Q_B site did not allow
283 the mediator (DQ) to accept electrons from the site and hence the process of electron transfer
284 from PS II to the mediator and further to the electrode was stalled. The detection was based on
285 the decrease in photocurrent in the presence of herbicides (see Frame B of Figure 3).

286 Reference photocurrent was first obtained without the addition of herbicides. A
287 preconditioning phase of about 10 minutes was required before the photocurrent from a fresh
288 biosensor became stable. A droplet (50 µl) of measuring buffer containing the mediator was
289 allowed to spread over the electrodes covered with immobilized PS II and the photocurrent
290 generated from the biosensor was measured for illumination time of 10 see after 10 min of
291 incubation. The biosensor was then subjected to successive droplets containing increasing
292 concentrations of the herbicide and the light-induced current was measured, again after 10 min of
293 incubation. In between applying different herbicide concentrations the sensor surface was
294 washed with excess of measuring buffer (including DQ) to remove the herbicide. Each
295 measurement was recorded three times at the same concentration of the analyte (using fresh
296 droplets) to check for reproducibility.

297 The data for different analytes was plotted as residual activity versus concentration (on a
298 logarithmic scale), Figure 7. The residual activity is the activity of the biosensor in percent after
299 addition of the inhibitor; it is equal to the ratio of photocurrents in the presence and in the
300 absence of the inhibitor. Experimental data were fitted to a logistic equation describing a
301 sigmoidal binding curve.

$$R = \min + \frac{Max - Min}{1 + (x/IC50)^H} \quad (1)$$

Here *Max* is the maximal activity before adding any analyte and *Min* is the minimum residual activity, when sensor is saturated by the inhibitor; *H* is the Hill slope, and *x* is the inhibitor concentration. The *IC50* is the point midway between top and bottom of the sigmoidal curve. The assumption behind the use of this curve is that the mediator and the inhibitor bind competitively to one and the same site on the PS II. The limit of detection, LOD, was calculated as

$$LOD = IC50 \left(\frac{2.6\sigma}{Max - Min - 2.6\sigma} \right)^{1/H} \quad (2)$$

see [28]. The factor of 2.6 corresponds to 99% confidence interval. Picric acid can be classified as nitrophenolic herbicide according to its chemical structure and has been employed in research on the feasibility of the PS II-based biosensors for explosives detection [28]. It has been previously described to be an inhibitor of PS II in photosynthetic electron transport [44]. The curve shifts towards higher concentrations for the picric acid in comparison to atrazine, indicating a lower degree of picric acid binding to the Q_B site. The fit parameters are presented in Table 2. The IC_{50} for picric acid is 15 times higher as compared to atrazine which signifies a lower affinity of picric acid for the Q_B binding site in comparison to triazine-type herbicides. The developed assay showed an excellent dynamic response range between 1 nM to 1 μ M for detection for atrazine and LOD is 1.15 nM indicating its potential application for environmental analysis. In repeated experiments, the reproducibility (coefficient of variation) of the sensor for $n=3$ measurements was $\sim 5\%$, for 10 nM atrazine concentration. The LOD of different atrazine sensors reported in the literature are summarized in Table 3. The limit of detection of 1.15 nM

324 for atrazine is significantly lower than the Maximum Residue Level (MRL) ($50 \mu\text{g L}^{-1}$ or 232
325 nM) established by EU (European Union) and close the MRLs for drinking water of each
326 individual pesticide at $0.1 \mu\text{g L}^{-1}$ and the total amount of pesticides at $0.5 \mu\text{g L}^{-1}$ (2.32 nM).
327 [Suggested location of Figure 7] For picric acid the sensor shows a relatively poor LOD of 157
328 nM which is mostly attributable to high σ . The LOD of ~ 25 nM has been reported for BSA
329 glutaraldehyde gel-immobilized PS II picric acid biosensor in [28]. The luminescence quenching
330 method yields LOD of $2 \mu\text{M}$ [45]; employing the fluorescence emission of hexaphenylsilole-
331 chitosan film the LOD of ~ 21 nM can be achieved [46]. It is important to point out that just like
332 most reported PS II-based herbicide biosensors [12,16,28], the one reported in this work is not
333 capable of distinguishing between different inhibitors without *a priori* knowledge of either the
334 nature of an inhibitor or the concentration. Thus, in its present form the biosensor is most
335 suitable for non-selective early-warning type applications. However, the use of genetically
336 modified PS II promises to allow better selectivity [18].

337 The main advantage of using SAM as compared to a matrix system is that due to smaller
338 biomolecule-to-electrode distance and to the absence of matrix which slows down the diffusion
339 of both analyte and the mediator, the equilibration and response times as well as the recovery
340 times are decreased, leading to lower illumination time being necessary. The peak response at
341 complete inhibition is near zero. It is possible to completely restore the signal by washing the
342 sensor with measuring buffer. The regeneration of the biosensor after experiments was almost
343 100% effective, in agreement with the results of [16]. It is also possible to reuse this sensor after
344 storage at 4°C within several hours, although within 24 hours the current drops substantially.
345 Longer-time storage of prepared sensors without loss of activity is possible at -80°C .

346

347 **Conclusions**

348 This paper investigates a method for covalent immobilization of photosynthetic reaction
349 centers on top of a defective self-assembled monolayer that allows mediator to access the surface
350 of the electrodes easily. The photocurrent generation properties in case of BBY particles were
351 compared to results obtained with BSA-glutaraldehyde matrix based immobilization and they
352 show faster rise and decay of the photocurrent upon switching illumination on and off, and better
353 signal to noise ratio. The pure preparations of Photosystem II cores (with no lipids) from spinach
354 leaves immobilize very nicely on the electrode surface but fair badly in terms of photocurrent
355 generation properties. The AFM investigations helped us to better understand some of the
356 obtained results as we see that BBY particles organize themselves into a layer structure on top of
357 the SAM leaving certain free spaces. The PS II core preparation in turn shows a very dense
358 organization with aggregate formation that leaves no space for mediator to access the electrodes.
359 The action of photosynthesis inhibitors in reducing photo-induced current was demonstrated for
360 atrazine and picric acid. The obtained detection limits were 1.15 nM and 157 nM, respectively.

361

362 **Acknowledgments:**

363 Authors are thankful to Dr. Rolf Schmidt, facility manager, Concordia University, for his help in
364 acquisition of AFM images and to Dr. C. Raman Suri (Pesticide Biosensors group) of IMTECH
365 Chandigarh, for fruitful discussions. The funding has been provided by NSERC under Strategic
366 Grants Program, Safety and Security. We acknowledge Defense R&D Canada, RCMP, CBSA
367 and CATSA as supporting organizations.

368

369

370 **References**

- 371 1. Z. Dai, H. Ju, *Phys. Chem. Chem. Phys.* 3 (2001) 3769-3773.
- 372 2. N.K. Chaki, K. Vijayamohanan, *Biosens. Bioelectron.* 17 (2002) 1–12.
- 373 3. S. Ferretti, S. Paynter, D.A. Russell, K.E. Sapsford, D.J. Richardson, *Trends Anal.*
- 374 *Chem.* 19 (2000) 530-540.
- 375 4. F. Frederix, K. Bonroy, W. Laureyn, G. Reekmans, A. Campitelli, W. Dehaen, G. Maes,
- 376 *Langmuir* 19 (2003) 4351–4357.
- 377 5. C.R. Suri, R. Boro, Y. Nangia, S. Gandhi, P. Sharma, N. Wangoo, K. Rajesh, G.S.
- 378 Shekhawat, *Trends Anal. Chem.* 28 (2009) 29-39.
- 379 6. B. Byrne, E. Stack, N. Gilmartin, R.O. Kennedy, *Sensors*, 9 (2009) 4407-4445.
- 380 7. I. Shitanda, S. Takamatsu, K. Watanabe, M. Itagaki, *Electrochim. Acta.* 54 (2009) 4933–
- 381 4936.
- 382 8. H. Peters, C.S. Dannert, R D. Schmid. *Mater. Sci. Eng. C* 4 (1997) 227-232.
- 383 9. S. Lemieux, R. Carpentier, *J. Photochem. Photobiol. B* 2 (1988) 221-231.
- 384 10. S. Lemieux, R. Carpentier, *Photochem. Photobiol.* 48 (1988) 115-121.
- 385 11. C. Loranger, R. Carpentier, *Biotechnol. Bioeng.* 44 (1994) 178-183.
- 386 12. D. Laberge, J. Chartrand, R. Rouillon, R. Carpentier, *Env. Toxicol. Chem.* 18 (1999)
- 387 2851-2858.
- 388 13. M. Koblížek, J. Masojídek, J. Komenda, T. Kucera, R. Pilloton, A. K. Mattoo, M. T.
- 389 Giardi, *Biotech. Bioeng.* 60 (1998) 664-669.
- 390 14. F. Bettazzi, L. Laschi, M. Mascini, *Anal. Chim. Acta* 589 (2007) 14–21.
- 391 15. E. Touloupakis, L. Giannoudi, S.A. Piletsky, L. Guzzella, F. Pozzoni, M.T. Giardi,
- 392 *Biosens. Bioelectron.* 20 (2005) 1984–1992.

- 393 16. M. Koblížek, J. Maly, J. Masojídek, J. Komenda, T. Kucera, M.T. Giardi, A.K. Mattoo, R.
394 Pilloton, *Biotechnol. Bioeng.* 78 (2002) 110-116.
- 395 17. A. Tibuzzi, G. Pezzotti, T. Lavecchia, G. Rea, M. T. Giardi, *Sens. Transducers* 88 (2008) 9.
- 396 18. K. Buonasera, G. Pezzotti, V. Scognamiglio, A. Tibuzzi, M.T. Giardi, *J. Agric. Food Chem.*
397 58 (2010) 5982-5990.
- 398 19. E.V. Piletskaya, S.A. Piletsky, T.A. Sergeyeva, A.V. El'skaya, A. A. Sozinov, J.L. Marty and
399 R.Rouillon, *Anal. Chim. Acta* 391 (1999) 1–7.
- 400 20. K.B. Lam, E.F. Irwin, K.E. Healy and L. Lin, *Sens. Act. B Chem.* 117 (2006) 480-487.
- 401 21. N. Terasaki, M. Iwai, N. Yamamoto, T. Hiraga, S. Yamada, Y. Inoue, *Thin Solid Films* 516
402 (2008) 2553–2557.
- 403 22. J. Maly, J. Krejci, M. Ilie, L. Jakubka, J. Masojidek, R. Pilloton, K. Sameh, P. Steffan
404 Z. Stryhal, M. Sugiura. *Anal. Bioanal. Chem.* 381 (2005) 1558–1567.
- 405 23. S. Campuzano, M. Pedrero, C. Montemayor, E. Fatas, J.M. Pingarron, *J. Electroanal. Chem.*
406 586 (2006) 112–121.
- 407 24. D.A. Berthold, G.T. Babcock, C.F. Yocum, *FEBS Lett.* 134 (1981) 231.
- 408 25. D.I. Arnon, *Plant Physiol.* 24 (1949) 1-15.
- 409 26. P.J. van Leeuwen, M.C. Nieveen, E.J. van de Meent, J.P. Dekker, H.J. Gorkom, *Photosyn.*
410 *Res.* 28 (1991) 149-153.
- 411 27. T. Hermanson, In: *Bioconjugate Techniques*, Academic Press, San Diego, CA, 1996, pp.
412 139–140.
- 413 28. V. Bhalla, X. Zhao, V. Zazubovich, *J. Electroanal. Chem.* 657 (2011) 84-90.
- 414 29. J. Shen, C.C. Liu, *Sens. Actuators B: Chem.* 120 (2007) 417-425.
- 415 30. O.A. Loaiza, S. Campuzano, M. Pedrero, J.M. Pingarron, *Electroanal.* 20 (2008) 1397–1405.

- 416 31. C.D. Bain, E.B. Troughton, Y.Y. Tao, J. Evall, G.M. Whitesides, R.G. Nuzzo, *J. Am. Chem.*
417 *Soc.* 111 (1989) 321-335.
- 418 32. V. Anandan, R. Gangadharan, G. Zhang, *Sensors* 9 (2009) 1295-1305.
- 419 33. V. Bhalla, S. Carrara, C. Stagni, B. Samorì, *Thin Solid Films* 518 (2010) 3360-3366.
- 420 34. Alcantara, B. Munge, Z. Pendon, H.A. Frank, J.F. Rusling, *J. Am. Chem. Soc.* 128 (2006)
421 14930–14937.
- 422 35. J. Maly, A. Masci, J. Masojidek, M Sugiura, R. Pilloton, *Anal. Letts.* 37 (2004) 1645-1656.
- 423 36. S. Carrara, V. Bhalla, C. Stagni, B. Samorì, *Surf. Sci.* 603 (2009) 75–77.
- 424 37. E. J. Boekma, B. Hankamer, D. Bold, J. Kruip, J. Nield, A. F. Boonstra, J. Barber, M.
425 Rogner, *Proc. Natl. Acad. Sci. USA* 92 (1995) 175-179.
- 426 38. A. Morrin, A. Guzman, A. J. Killard, J. M. Pingarron, M. R. Smyth, *Biosens. Bioelectron.* 18
427 (2003) 715–720.
- 428 39. M. Vittadello, M.Y. Gorbunov, D.T. Mastrogiovanni, L.S. Wielunski, E.L. Garfunkel, F.
429 Guerrero, D. Kirilovsky, M. Sugiura, A.W. Rutherford, A. Safari, P.G. Falkowski,
430 *ChemSusChem* 3 (2010) 474-475.
- 431 40. R. Ganapathy, S. Manolache, M. Sarmadi, W. J. Simonsick Jr., F. Denes, *J. Appl. Polym.*
432 *Sci.* 78 (2000) 1783–1796.
- 433 41. Z. Naal, J.H. Park, S. Bernhard, J.P. Shapleigh, C.A Batt, H.D. Abrua, *Anal. Chem.* 74
434 (2002) 140–148.
- 435 42. R.D. Richins, A. Mulchandi, W. Chen. *Biotechnol. Bioeng.* 69 (2000) 591–596.
- 436 43. M. Darder, E. Casero, F. Pariente, E. Lorenzo, *Anal Chem.* 72 (2000) 3784–3792.
- 437 44. W. Oettmeier, K. Masson, *Eur. J. Biochem.* 122 (1982) 163-167.
- 438 45. J. Lu, Z. Zhang, *Anal. Chim. Acta.* 318 (1996) 175.

- 439 46. G. He, H. Peng, T. Liu, M. Yang, Y. Zhang, Y. Fang, *J. Mater. Chem.* 19 (2009) 7347.
- 440 47. S. Hleli, C., Martelet, A. Abdelghani, N. Burais, N., Jaffrezic-Renault, *Sens. Actuators B* 113
- 441 (2006) 711–717.
- 442 48. E. Valera, J. Ramón-Azcón, F.-J. Sanchez, M.-P. Marco, Á. Rodríguez, *Sens. Actuators B*
- 443 134 (2008) 95-103
- 444 49. J. Přibyl, M. Hepel, J. Halamek, P. Skladal, *Sens. Actuators B* 91 (2003) 333–341.
- 445 50. C. Steegborn, P. Skladal, *Biosens. Bioelectron.* 12 (1997) 19-27.
- 446 51. C.R. Suri, J. Kaur, S. Gandhi, G.S. Shekhawat, *Nanotechnology* 19 (2008) 235502.
- 447 52. R. Wilson, M.H. Barker, D.J. Schiffrin, R Abuknesha, *Biosens. Bioelectron.* 12 (1997) 277–
- 448 286.
- 449 53. J. Kaur, R.C.Boro N. Wangoo, K. Rajesh, C.R. Suri, *Anal. Chim. Acta.* 607 (2008) 92-98.
- 450

451 **Figure Captions**

452

453 **Figure 1.** Schematics of the biosensor employed in this work. PS II-containing particles are
454 immobilized on top of a defective monolayer of MPA on a gold electrode. Light induces charge
455 separation in PS II and after several steps the electrons are accepted at the Q_B binding site by a
456 non-native quinone (duroquinone, DQ) The reduced DQ leaves the Q_B site and is eventually
457 oxidized at the gold SPE and the photo-induced current is detected. Introduction of
458 photosynthesis inhibitors interrupts this chain of events and the photoinduced current is reduced.

459

460 **Figure 2.** CV scans obtained using 30 mM ferrocyanide in measuring buffer (no DQ) for bare
461 Au-SPE (solid curve) and after MPA SAM formation (dashed curve). The scan rate was 50 mV

462 | see⁻¹.

463

464 **Figure 3.** Comparison of photocurrent signal from BBY particle biosensor in case of (A) BSA-
465 glutaraldehyde matrix immobilization and (B) immobilization onto a self-assembled MPA
466 | monolayer in the absence of inhibitors, solid curves. The illumination time is 20 see for (A) and
467 | 10 see for (B). The dotted curve in frame B is the photocurrent peak in the presence of an
468 | inhibitor, superimposed on the figure for illustrative purposes.

469

470 | **Figure 4.** AFM images. Square side is $5.0 \mu\text{m}^2$. a) Bare gold surface and b) Gold surface after
471 | formation of MPA SAM. In the image (b), the brighter regions correspond to the condensed
472 | thiol islands (liquid or solid phase), and the darker regions correspond to the dilute phase (bare
473 | Au surface).

474

475 | **Figure 5.** AFM images of PS II particles immobilized on a MPA monolayer; square size 2.5
476 | μm^2 . a) PS II cores from spinach. Immobilized particles show cluster formation thus blocking
477 | mediator access to the electrode surface; b) BBY particles: immobilized particles as well as
478 | access sites to electrodes are visible. The RMS roughness in the highlighted square region is 4.16
479 | nm. Below the AFM images the respective schematic drawings of the biolayers are presented.

480

481 | **Figure 6.** Cross-sectional views along the lines present in Figure 4. a) PS II core particles are
482 | located right next to each other and some aggregates are formed. b) Highly disordered situation
483 | in case of BBY membranes, with grooves clearly spanning the whole thickness of the biolayer.

484

485 | **Figure 7.** Calibration curves for the decrease of photocurrent upon addition of picric acid (open
486 | circles) and atrazine (solid circles) in the presence of 0.2 mM DQ. The experimental points were
487 | fitted using Eq.1.

Table 1. RMS roughness for various samples/surfaces

Sample	RMS roughness in nm for 2.5 μm^2 square
Bare evaporated gold	1.05 \pm 0.1
MPA-SAM	1.85 \pm 0.25
PS II cores	21.9
BBY	8.67

Table 2. Fitting parameters (Eqs. 1 and 2) for picric acid and atrazine

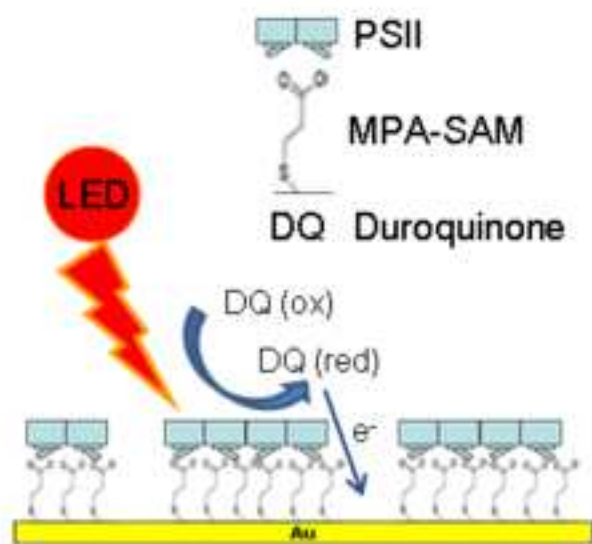
	Min (%)	Max (%)	EC50 (nM)	σ	Hill slope	R^2	LOD (nM)
atrazine	7.6	100.0	49	1.57	0.82	0.9984	1.15
picric acid	10.4	100.0	784	4.83	1.13	0.9936	157.5

Table 3. Examples of atrazine biosensors

Ref.	Methodology	LOD
[47]	Impedimetric, label-free immunosensor	20 ng/ml 93 nM
[48]	Impedimetric, label-free immunosensor	8.34±1.37 ng/ml 39 nM
[49]	Piezoelectric, label-free immunosensor	1.5 ng/ml (direct) 7 nM / 0.025 ng/mL (competitive) 0.11 nM
[50]	Piezoelectric	0.1 µg/l 0.46 nM
[51]	Nanomechanical Cantilever based	pM
[52]	Electrochemiluminescence flow injection immunoassay	0.1 ppb 6 nM
[53]	Direct hapten coating microtiter plates	20 ng/L 0.09 nM
This work	PSII biosensor	247 ng/L 1.15nM

Figure

[Click here to download high resolution image](#)



Figure

[Click here to download high resolution image](#)

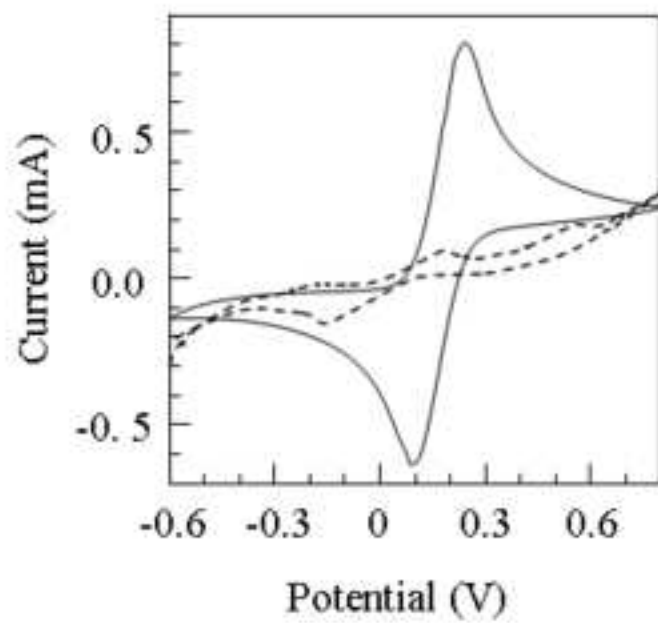


Figure 2

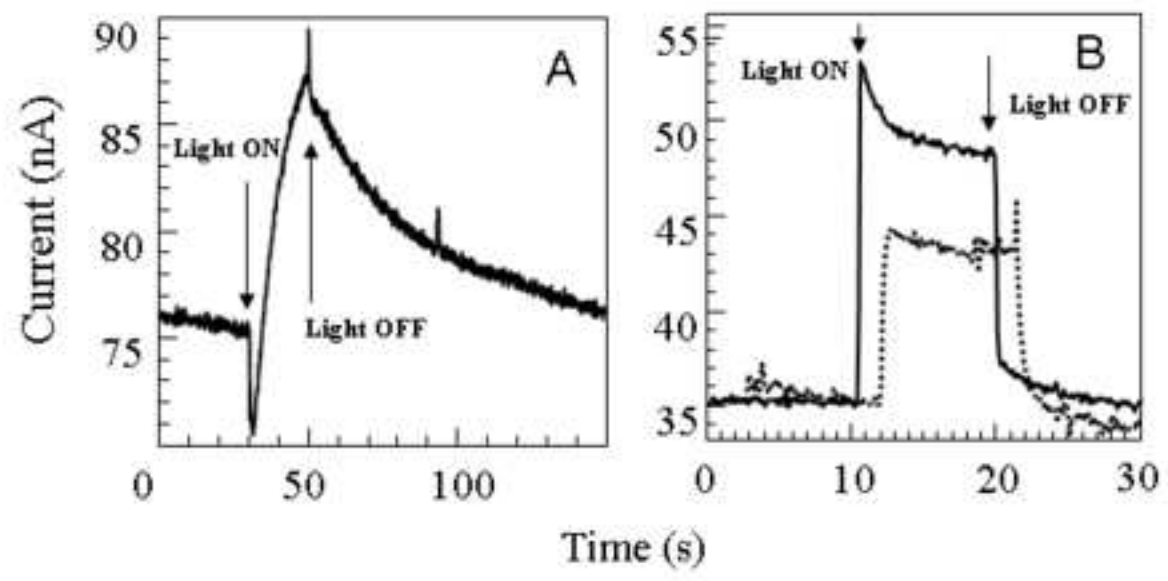


Figure 3

Figure
[Click here to download high resolution image](#)

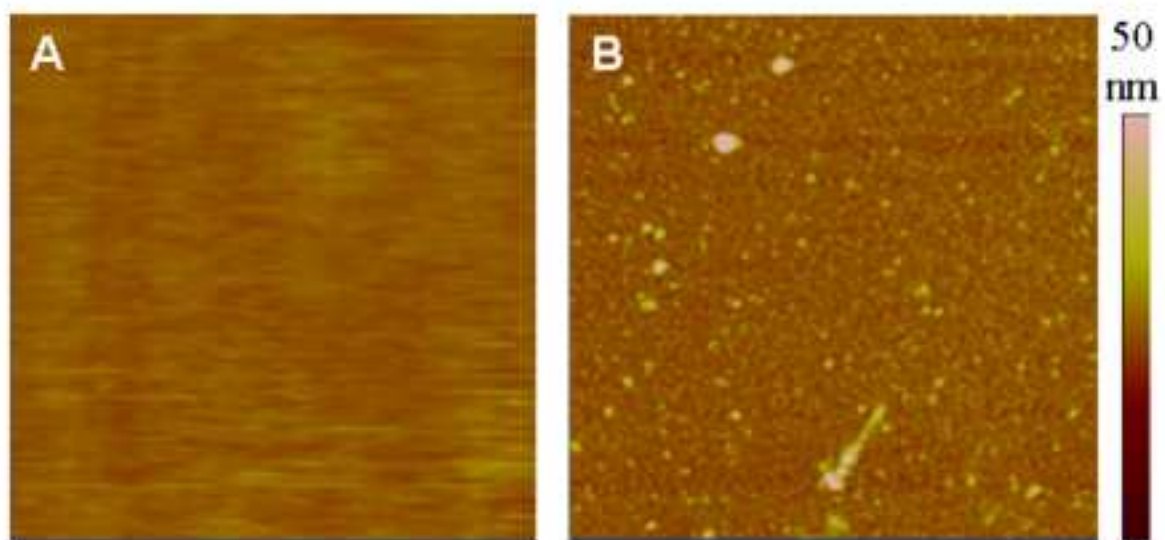


Figure 4

Figure
[Click here to download high resolution image](#)

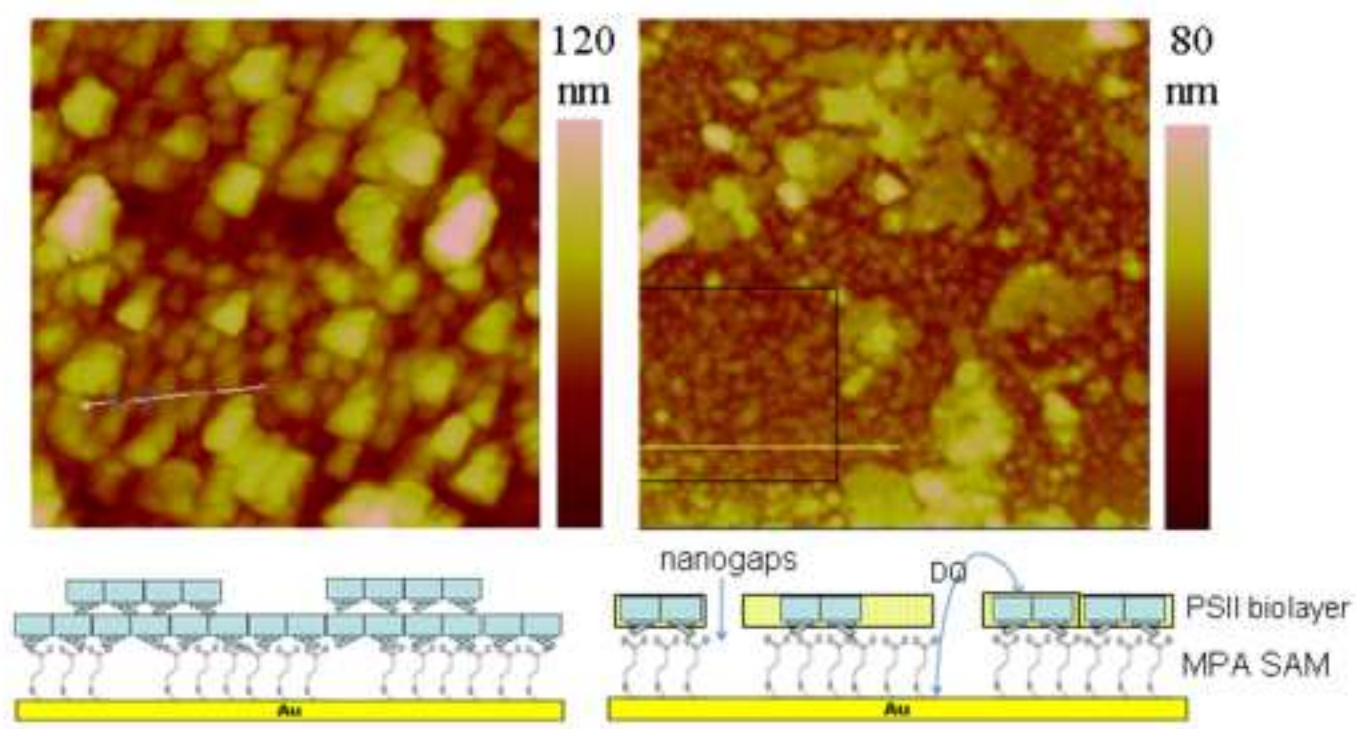


Figure 5

Figure
[Click here to download high resolution image](#)

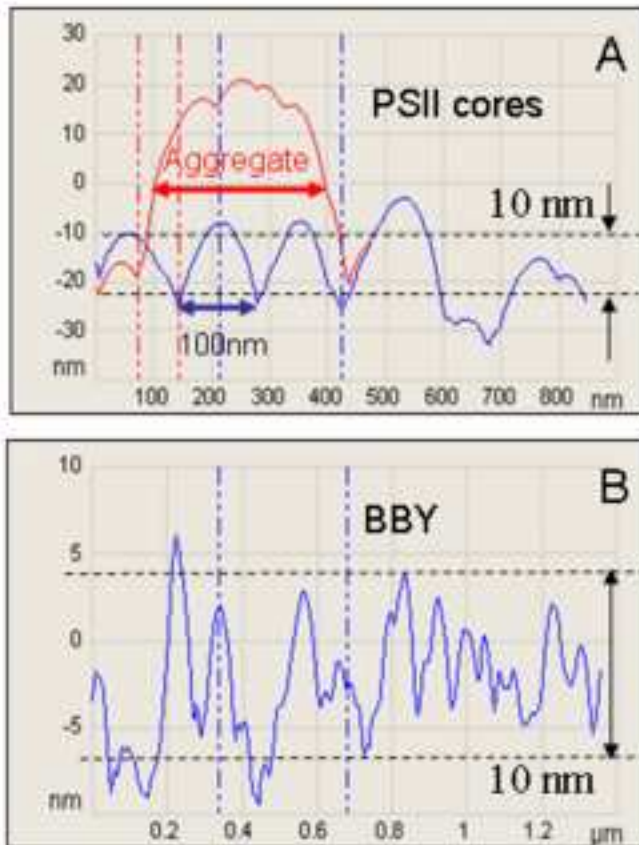


Figure 6

Figure

[Click here to download high resolution image](#)

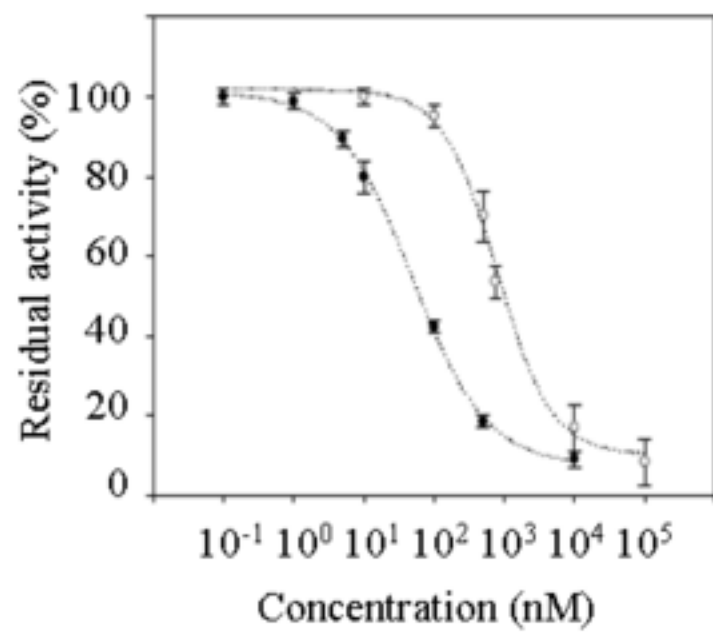


Figure 7

Electronic Supplementary Material (online publication only)

[Click here to download Electronic Supplementary Material \(online publication only\): Supplementary Information.doc](#)